Jurnal Tribologi 46 (2025) 32-57

MYTRIBOS Malaysian Tribology Society

Jurnal Tribologi

Website : jurnaltribologi.mytribos.org e-issn: 2289-7232

Railway curve squeal analysis using complex eigenvalue

Charvinder Singh [1], Zaidi Mohd Ripin [1*], Nurul Farhana Mohd Yusof [1], Mohd Fauzinizam Razali [1], Muhammad Najib Abdul Hamid [2]

[1] The Vibration Lab, School of Mechanical Engineering, Universiti Sains Malaysia, MALAYSIA.
[2] Kampus Malaysian Spanish Institute, Universiti Kuala Lumpur, MALAYSIA.
[*]Corresponding author: mezaidi@usm.my

KEYWORDS

Contact point
Finite element (FE)
Friction coefficient
Complex eigenvalue
Instability
Real and imaginary parts
Unstable modes

ABSTRACT

High-frequency noise of railway curve squeal is a multifaceted phenomenon produced by the interaction between the train wheel and curved track. In this study, an experimental rig was developed to study the interaction of the wheel and track using twin-disk mechanism. A finite element model was developed to represent the system, and complex eigenvalue analysis was performed for the twin-disk system. The model's mode shapes and frequency matched those of the experimental modes within 10%. To simulate the effect of curvature, the system was preloaded laterally and subjected to a 3° rotational motion around the vertical axis. The detected positive real part of the eigenvalues denotes instability. The results showed that for the baseline friction coefficient μ = 0.35, the unstable eigenvalues were 1086, 2312, and 4300 Hz. The unstable modes corresponded well with the measured squeal frequency of 2400 Hz, validating the two-disc model. A parametric analysis was conducted to assess the impact of operating parameters such as friction coefficient, preloading, and wheel contact positions. The findings indicated that the wheel–rail system exhibited instability when the friction coefficient exceeded μ = 0.35, and that contact at the field side and a yaw angle more than 0.5° exacerbated instability.

Received 2 October 2024; received in revised form 9 January 2025; accepted 22 April 2025.
To cite this article: Singh et al. (2025). Railway curve squeal analysis using complex Eigenvalue. Jurnal Tribologi 46, pp.32-57.

1.0 INTRODUCTION

When a train travels on a curved track, it produces a periodic high-frequency noise known as squeal. Curve squeal typically manifests at track curve radii between 400 m and 800 m (Lee & Kim, 2011), with a squealing frequency reported between 4000 and 10000 Hz (Sueki et al., 2022) emanating from the leading wheelset (Vincent et al., 2006). This squealing phenomenon significantly impacts railway infrastructure, which becomes more susceptible to wear and damage. As indicted by (Hanson et al.,2014) a curve radius below 300m results in the wrapping of a 3-piece bogie due to elevated rail stresses incurred during curve negotiation. Bogies exhibiting a high wear rate were found to have an unevenness exceeding 16 mm, a condition that causes warping and limits the wheel's lifespan to a maximum of 5 years, compared to the standard wheel life of 9 years (Valente et al., 2023). Ma and Yang (2024) indicated that rail corrugation, a periodic wear of the rail surface, develops more prominently on smaller curves due to increased creepage in the contact region. This observation aligns with Chen's (2020) study, which noted that curved tracks with a radius of curvature less than 350m are prone to rail corrugation, with an occurrence probability nearing 100%. In contrast, curves with a radius exceeding 650m account for only 0.1-0.5% of corrugation development (Chen, 2020). According to Wang et al. (2024) rail corrugation induces fatigue wear, leading in the fracture of the rail structure, including fasteners, track plates, and sleepers, as well as the initiation of cracks in the subsurface of the rail. This damage will impede the efficient running of the train and result in increased maintenance costs and workload to maintain the railway infrastructure. Besides that, it also affects passengers traveling on the train and nearby residents. Furthermore, residents living close to curved tracks are subject to adverse health effects, including an increased risk of cardiovascular disease, as reported by Münzel et al. (2024). Prolonged exposure to transportation noise can disrupt sleep patterns, leading to high blood pressure—a primary factor contributing to cardiovascular issues (Münzel et al., 2024). Long-term exposure to railway noise has also been associated with a 26% increased likelihood of cognitive impairment in older adults (Wu et al., 2024). Therefore, it is essential to reduce the noise level to minimize potential harm to both passengers and nearby residents.

Beshbichi et al. (2020) reported that rail curvature is characterized by a quasi-sinusoidal irregularity at the railhead. This issue, resulting from the small radius of curvature, is prevalent across nearly all rail lines (Beshbichi et al., 2020). The coefficient of friction, contact sites, and the rigidity of the rail support springs contributes to the generation of curve squeal noise (Goo & Kim, 2016). The finite element (FE) method, particularly through complex eigenvalue analysis, is commonly used to understand the mechanics of railway curve squeal (Chen et al., 2008). Complex eigenvalue analysis is the most extensively applied frequency domain approach for examining railway curve squeal (Thompson et al., 2018). The finite element method yields results that are comparable to experimental findings (Ghani et al., 2024).

The curve squeal phenomenon is primarily attributed to two fundamental mechanisms: falling friction and mode coupling. Multiple hypotheses have been proposed and examined to elucidate the generation of squeal noise mechanism. RUDD and Bolt Beranek and Newman Inc. (1976) demonstrated that the stick-slip phenomenon in the contact region is the primary contributor to squeal, based on a model of lateral crabbing of wheels on railheads. According to Goo (2014), stick-slip occurs due to a reduction in the friction coefficient with slippage. This phenomenon can result in negative damping in a structure and induce self-excited, unstable vibration (Goo, 2014). Xie et al. (2006) extended the model by De Beer et al. (2003) and performed a steady-state curving analysis that incorporated falling friction on curve radii. They found that the occurrence of squeal

is significantly influenced by curve radius, with falling creep forces observed at the outer and inner front wheels, particularly at radii between 150 m and 250 m. However, the rear wheel did not exhibit squealing, as the lateral creep force threshold was not reached (Xie et al., 2006). Rusli et al. (2020) emphasized the importance of nonlinear contact models in analyzing squeal generation, revealing that stick-slip and mode-coupling occur concurrently, producing squeal as the coefficient of friction and contact force increase. Heckl and Abrahams (2000) used a time-domain model representing the wheel as a flat circular surface, applying stick-slip friction to create interaction, and demonstrated that crabbing speed determines the amplitude limit cycle velocity, which governs the intensity of squeal emanating from the wheel's unstable mode. However, this study was later extended in the frequency domain to determine the stability of individual modes (Heckl, 2002).

Mode coupling is a well-known phenomenon in the field of automotive brake squeal (Du & Wang, 2017). For mode coupling to occur with constant friction, as noted by Glocker et al. (2009), the normal and tangential directions must be coupled in the contact region, leading to self-excited vibration. Meehan (2019) presented a mathematical and complex eigenmode model that incorporated both mode coupling and falling friction, showing that viscous mode coupling amplified squeal by up to 5 dB under high rail damping for the outer wheel. Ding et al. (2018) introduced falling friction using Huang's (2007) model alongside constant friction and demonstrated that mode coupling offset and contact angle affected squeal, showing that mode coupling occurs in both the inner and outer wheels. A parametric investigation of friction-induced vibration indicated that changes in mass, stiffness, and friction coefficient significantly influenced the eigenvalues of the wheel-rail system, providing key insights into the structural instability of the system (Inoue & Kamada, 2020). Gao et al. (2023) examined the parameters influencing wheel-rail curve squeal noise, with a focus on stiffness matching, and found that unstable modes are closely associated with the resonance frequency and mode shape of the wheel and rail.

Empirical validation of a theory is essential. Koch et al. (2006) constructed a reduced rig model, scaled to a quarter of the actual size. Squeal is produced when the angle of attack exceeded 8 mrad and the friction coefficient was above 0.3μ under dry conditions. However, it was found that vertical loading and lateral contact did not cause squealing (Koch et al., 2006). Hsu et al. (2007) designed a twin-disc rig capable of measuring lateral force, which is useful for assessing lateral vibration at the contact patch. However, the study reported that third-body abrasive behavior should be examined, as it causes inaccuracies in adhesion coefficients. Notably, the rig has a limited yaw angle adjustment of only 2.5 °, which does not account for larger yaw angles (Hsu et al., 2007).

Numerous investigations seeking to elucidate the phenomenon of rail curve squeal have been reported. The findings from these studies highlight the importance of finite element analysis in identifying and addressing the causes of squealing on curved tracks. However, most studies have not considered the effects of yaw angle by preloading the system in the vertical and lateral directions, thus overlooking the impact of curving on the system instability based on these parameters.

In this study, mode coupling was assumed to be the primary cause of squeal. A twin-disc rig with an adjustable yaw angle was developed to examine wheel-rail interaction, and this setup was validated against a twin-disc finite element model that simulates the wheel-rail system with a friction contact interface. Complex eigenvalue analysis was then conducted to assess the effects of vertically and laterally preloading the wheel-rail system at varied yaw angles, simulating a curved track. A parametric analysis was performed to evaluate the impact of contact position and

friction coefficient on system instability, which manifests as squeal. In this regard, the system stability can be analyzed using complex eigenvalue analysis, with the positive real part serving as a measure of instability.

2.0 METHODOLOGY

2.1 Development of Finite Element Model

Figure 1 shows the wheel-rail system, which comprises two disks. The track is represented by the disk with the larger diameter, and the wheel is represented by the disk with the smaller diameter. Abaqus 6.13 was utilized to construct the FE model, and both disks were entirely designed within their Abaqus native environment. The FE model used for simulation is a linear model. The mechanical parameters of the model are listed in Table 1. Both the wheel and rail were made from steel, with the rail geometry based on the UIC 60 rail standards, while the wheel design was based on S1002 standards, the dimensions used are illustrated in Figure 2 and Figure 3, which are at a scale of 1:3 of the actual model. Both the wheel and track were represented as solid deformable structures exhibiting complete elasticity. The axes X, Y and Z represents the lateral, vertical and rolling direction, respectively.

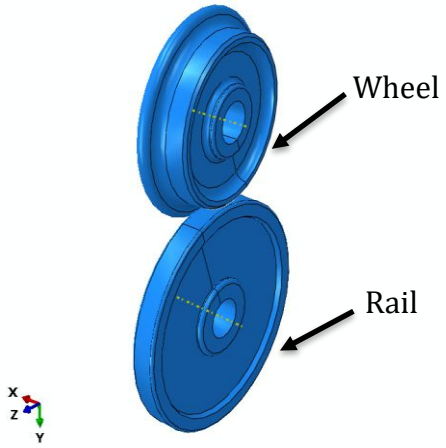

Figure 1: Finite element model.

Table 1: Mechanical parameters of the FE model.

Young's Modulus, E	210 GPa
Yield Strength	545 MPa
Poisson's Ratio	0.3
Density	7590 kg/m^3

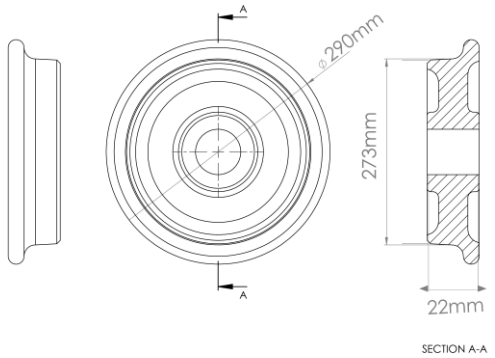

Figure 2: Wheel dimensions in mm.

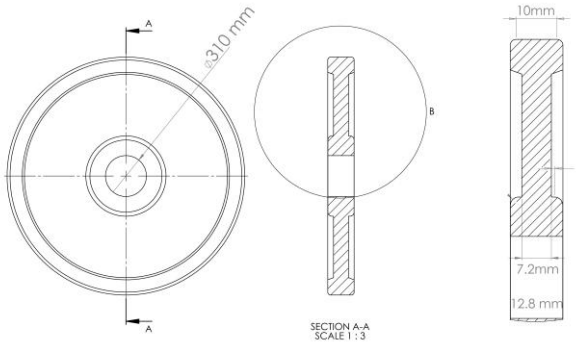

Figure 3: Rail dimensions in mm.

2.1.1 Mesh Convergence

A mesh convergence study was performed before the complex eigenvalue analysis. Using a finer mesh in FE analysis is crucial since it leads to more precise outcomes without increasing the computing load. Eight convergence runs were undertaken to obtain the relationship (Figure 4) between contact pressure and element size at the contact region. Once point F is reached, further mesh refinement has little impact on the contact pressure. The contact region at point F has an element size of 0.6 mm and a maximum contact pressure of 500 MPa. Therefore, 0.6 mm was selected as the optimal mesh size. The wheel-rail system was simulated using 32122 linear hexahedral (C3D8I) elements with 38982 nodes. Hidayat et al. (2023) stated that the primary criterion for generating accurate and reliable results is significantly dependent on the optimal mesh model, without compromising the computational load during finite element analysis. Coarse elements with less than 5000 elements may yield inaccurate results, while it was noted that hexahedral element model produced more accurate results compared to tetrahedral element as evidenced in investigation of mesh model for prosthetic hip joint using finite element analysis (Hidayat et al., 2023).

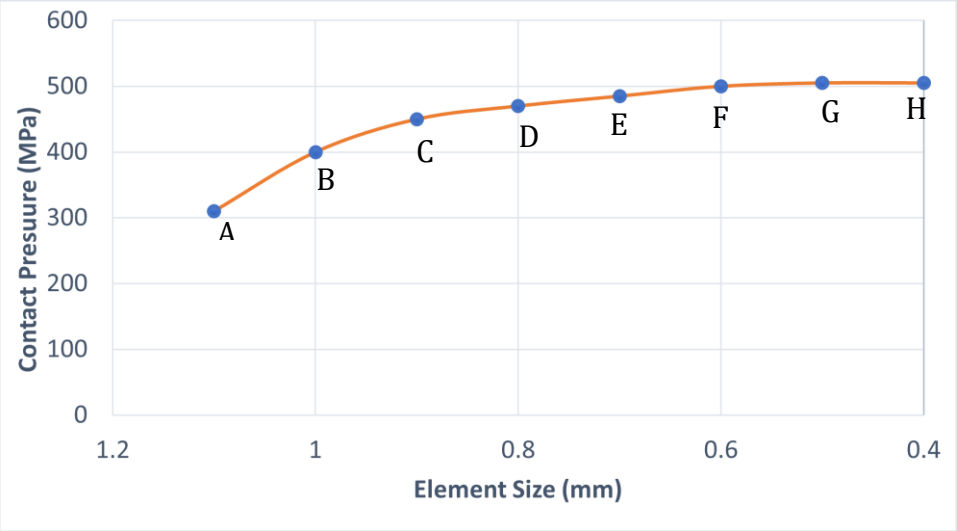

Figure 4: Convergence of contact pressure with mesh size.

2.1.2 Modeling the Radius of Curvature Effect

To illustrate the dynamics of curving motion and the effects of yaw angle when navigating a curve to accomplish curve effect, four steps were performed, as follows:

Step 1: Preloading of wheel–rail system

Curve squeal effects is simulated by preloading in the radial, rotational, and lateral directions. To simulate curved track squealing, a preload force of 1500 N is applied to the rail in the lateral direction, and a force of 1500 N is applied to the wheel in the vertical direction, as shown in Figure 5. The system is preloaded to maintain similar stress levels in both the forward and lateral orientations throughout curving motion. The vertical force exerted in this study functions as a normal load. A vertical force of 1500 N is applied to establish a Hertzian conformal contact between the rail and wheel, resulting in a contact patch with a maximum contact pressure of 500 MPa. According to Hsu et al. (2007) and Anyakwo (2020b), a normal load ranging from 500 N to 2200 N is adequate for conducting curve squeal experiments on the test rig to simulate actual track conditions. Hence, a normal load of 1500 N was selected as ideal to induce curve squeal on a twin disk rig, aligning with the literature. Whereas the lateral force applied in this study serves as an accurate indicator for the occurrence and intensity of squeal, as demonstrated by Pieringer (2014b) in her time domain analysis. The parametric study, as illustrated in Figure 18, confirms the claim by demonstrating that the system's instability increases in proportion to the lateral load. Moreover, as noted in the literature, a lateral force of 1770 N applied at the wheelset to replicate a curve was found to initiate squeal, representing 16% of the value utilized in this study (Giner-Navarro et al., 2018). Thus, the 1500 N lateral force employed in this study is sufficient to induce a squeal.

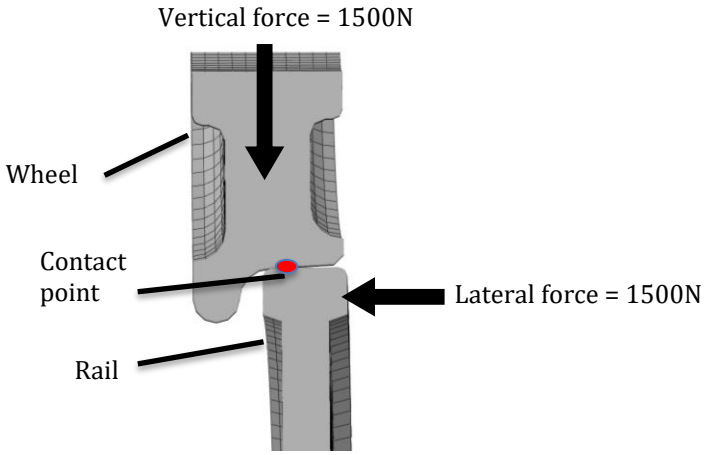

Figure 5: Cross-section of the wheel–rail profile.

The surface-to-surface approach is then employed to establish interaction between the wheel and rail, with a baseline friction coefficient of μ = 0.35. The secondary surface is the rail, while the primary surface is the wheel. The discretization approach was set to surface-to-surface, and a small-sliding contact algorithm was employed. Tangential behavior was implemented in conjunction with the penalty approach. To accurately analyze the squeal phenomenon, contact behavior is essential in the analysis of curving dynamics.

Step 2: Inducing curvature effect

The wheel is subjected to a yaw angle with a baseline value of 0.5 °. This is achieved by rotating the wheel around the vertical axis (Y axis) to simulate the effects of radial curvature on the tendency of the wheel to squeal. The wheel is rotated around the vertical axis with the baseline value and then varied until 3° to demonstrate the dynamics of curving motion and the impact of yaw angle when navigating a curve. A study conducted by Yun and Kim (2021) demonstrated that the highest adhesion coefficient is achieved at a yaw angle of 0.5°; as the yaw angle exceeds 0.5°, the adhesion coefficient decreases, leading to instability defined by significant squeal noise in the twin disk rig (Yun & Kim, 2021). Therefore, a baseline yaw angle of 0.5° was selected for this study. However, due to the limitations of our twin-disk rig, the yaw angle can be adjusted only to a maximum of 3°. Owing to the horizontal position of the rail, the axis of rotation results in a yaw angle between the wheel and rail. The curvature effect can be replicated by measuring the lateral effect, that is, the difference in tangential rolling velocities of the wheel and rail. In this scenario, the fundamental cause of instability is the negative correlation between friction coefficient and sliding velocity.

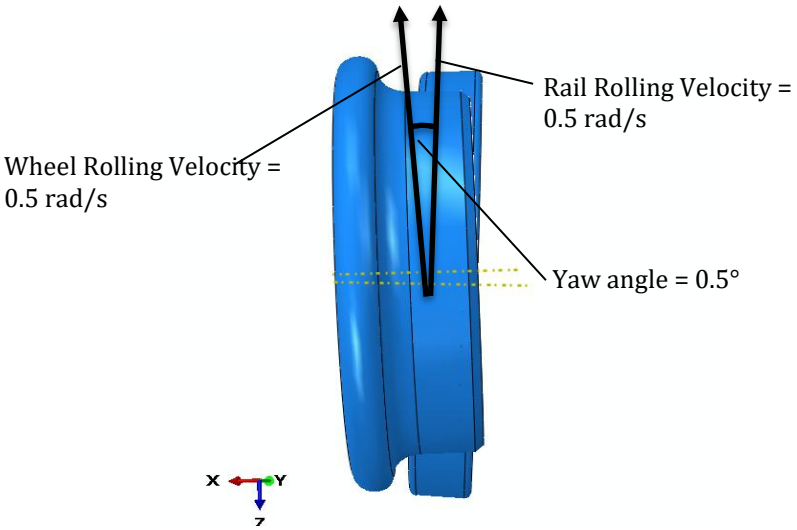

Figure 6: Top-view of wheel–rail profile.

Step 3: Employing boundary conditions

Rolling conditions were established by implementing displacement/rotation-type boundary conditions to enforce rotational movement on the wheel and track. The wheel and rail were subjected to an angular velocity of 0.5 rad/s as exceeding this threshold necessitates substantial computational resources and time. Displacement/rotation type boundary conditions were used. All degrees of freedom and orientations in the rotational and translational directions were strictly constrained for the wheel and rail, except for UR1, which denotes rotational motion along the X-axis to facilitate the rolling effect of the wheel and rail, and U2, which represents translational motion along the Y-axis to accommodate a vertical load of 1500N.

For this stage, the keywords are modified to "*MOTION, ROTATION." This is essential because in the analysis, the nodes of a structure lack any flexibility to move. Consequently, boundary conditions such as rotation or displacement cannot be implemented without modifying the keywords.

Step 4: Complex Eigenvalue analysis

The system's resonant frequency was extracted through modal analysis conducted under free-free conditions before the complex eigenvalue analysis. In this stage, the unstable modes and eigenvalues were extracted in DAT file format. Parametric studies were subsequently performed to evaluate the effects of increasing the friction coefficient, shifting the contact point, and altering the yaw angle.

2.2 Experimental Setup

A twin-disk rig depicted in Figure 7, using the same dimensions as the FE model, was developed to validate the finite element model and to examine the behavior of the rail-wheel system during curves, with particular emphasis on the unstable vibrations induced by friction. The dimensions are presented in Section 2.1.A 10 kW three-phase induction motor was used to control the speed of the wheel. The track was linked to a turntable and the yaw angle could be adjusted up to 3° to replicate the state of lateral sliding. The data acquisition system from National Instruments was used to measure the squealing, vibration mode, and noise level. The LMS TestLab

equipment was used to assess the squeal modes and noise frequency components as shown in table 2. The squeal measurement was performed in a controlled laboratory setting, with accelerometers positioned at the frame. To prevent motor noise, an integrated-circuit piezoelectric (ICP) microphone was put 100 mm away from the setup. The measurement was conducted with the wheel's rolling speed adjusted to 500 rev/m by the motor, as indicated in the studies of X. Liu and Meehan (2013) and, X. Liu and Meehan (2013b) which indicated that a rpm level over 400 rev/m resulted in a significant squeal with a sound pressure level exceeding 100 dB. Thus, the optimal rpm chosen for this study was 500 rev/m, as increasing the rpm beyond this level resulted in significant wear to the wheel and rail.

Figure 7: Twin-disk rig.

3.0 RESULTS AND DISCUSSION

3.1 Model Validation

In this study, both the FE model and the experimental model have the same dimensions and scale, at a ratio of 1:3 of the actual size. To validate the precision of the FE model, the natural frequency derived from the FE modal analysis is compared with the data from the literature that employs the same dimensions and scale, therefore verifying both the FE model and the experimental model. The comparison is depicted in Tables 2 and 3. The dimensions, materials, and setup utilized in the literature align with those implemented in this study.

In order to obtain the mode shapes in their natural state, free–free modal analysis was performed with no boundary conditions imposed on the wheel and rail. The error percentage was then calculated and displayed for each mode in comparison to the experimental mode, as shown in table 4. Whereas both the modes shapes of the FE model and experimental model were contrasted as in Figures 8 and 9. The modes exhibited comparable shapes, and the error percentage remained less than 10%. Therefore, the FE model was a valid representation of the physical model.

Table 2: Wheel validation against literature.

Wheel			
Mode	**Literature (Hz) Anyakwo (2020b)**	**Actual Study (Hz)**	**Error (%)**
1	2868	2890	0.70
2	5225	4715	9.76
3	7956	7743	2.67

Table 3: Rail validation against literature.

Rail			
Mode	**Literature (Hz) Anyakwo (2020b)**	**Actual Study (Hz)**	**Error (%)**
1	3128	3470	10.93
2	5520	4559	17.40
3	8360	7508	10.19

Table 4: Free-free modal analysis of FE and experimental model.

	Wheel			**Rail**		
Mode	**FE model (Hz)**	**Experimental Model (Hz)**	**Error %**	**FE model (Hz)**	**Experimental Model (Hz)**	**Error %**
1	2890	3180	9.11	3470	3209	8.13
2	4715	4397	7.23	4559	4397	3.66
3	7743	8186	5.14	7508	6945	8.16

Wheel	
FE model	Experiment Model
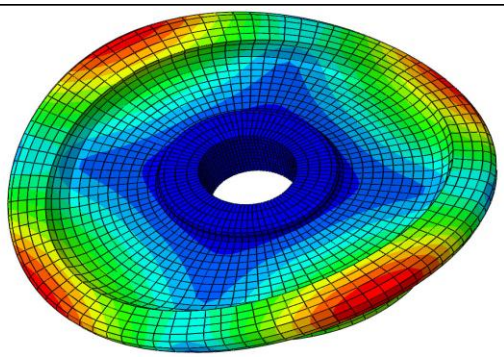 **Mode 1: 2890 Hz**	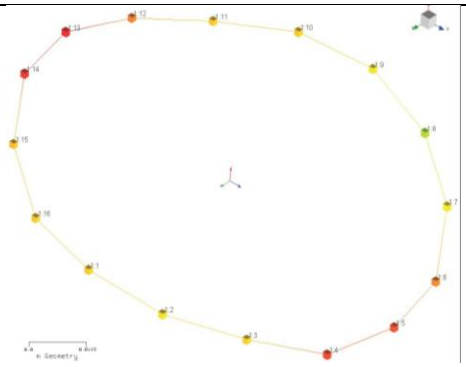 **Mode 2: 3180 Hz**
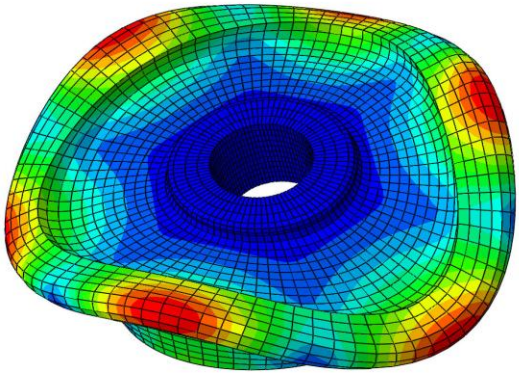 **Mode 2: 4715 Hz**	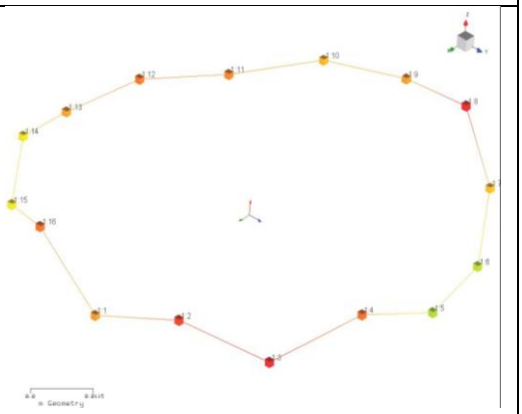 **Mode 2: 4397 Hz**
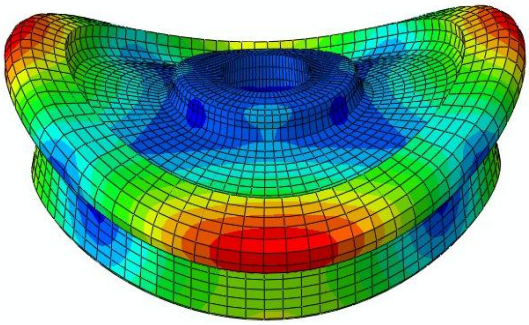 **Mode 3: 7743 Hz**	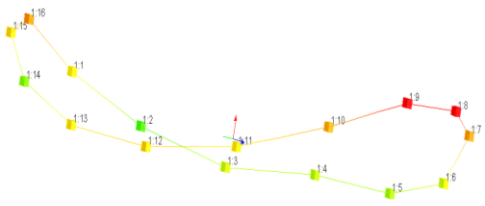 **Mode 3: 8186 Hz**

Figure 8: Wheel mode shapes.

Rail	
FE model	Experiment Model
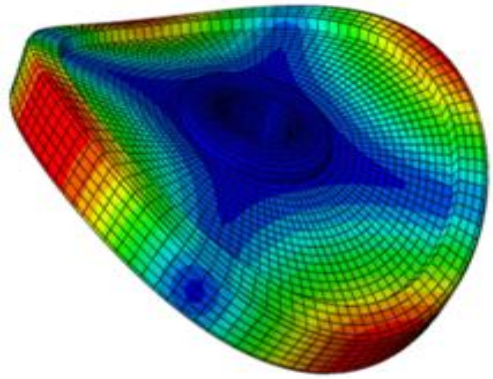 **Mode 1: 3470 Hz**	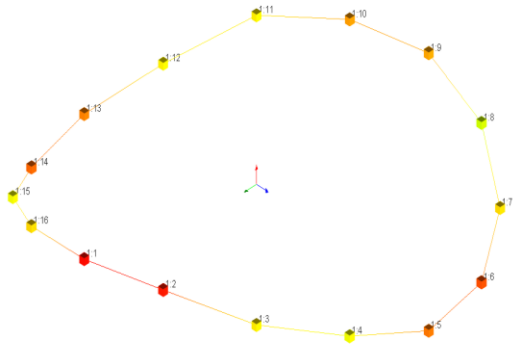 **Mode 1: 3209 Hz**
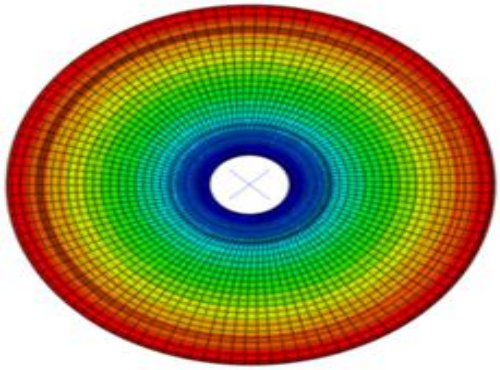 **Mode 2: 4559 Hz**	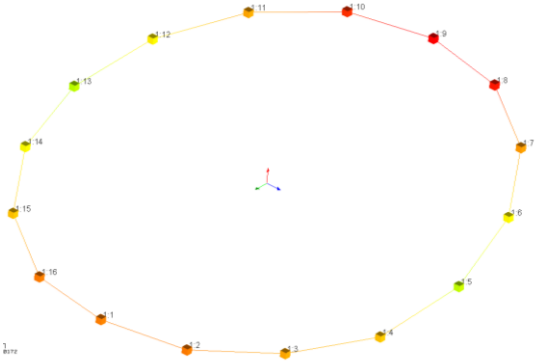 **Mode 2: 4397 Hz**
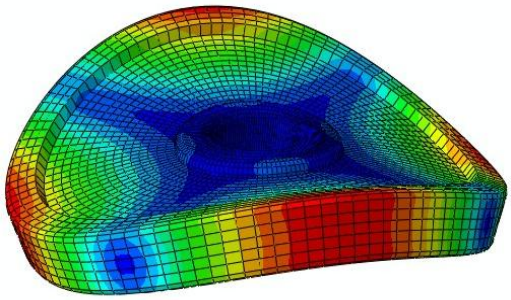 **Mode 3: 7508 Hz**	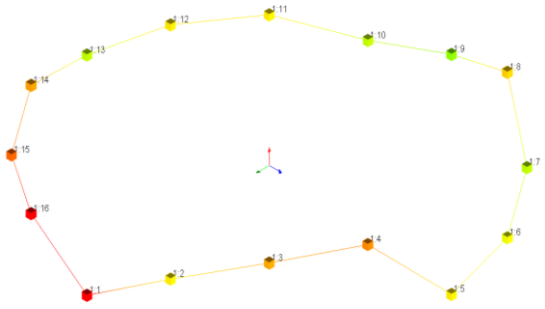 **Mode 3: 6945 Hz**

Figure 9: Rail mode shapes.

3.2 Stability Analysis

Complex eigenvalue analysis was performed to extract and assess the unstable vibration modes of the wheel-rail system caused by self-excited vibrations induced by frictional contact. The coefficient of baseline friction was set to μ = 0.35 based on the absence of unstable modes below μ = 0.35, as shown in Figure 8(see section 3.3).

Table 5 lists the eigenvalues obtained from the complex eigenvalue analysis. The table shows mode number, real part, and the corresponding frequency. A total of six eigenmodes were identified, with each positive real part paired with the corresponding negative real part. When a real component has a conjugated series, it implies that the corresponding frequency will merge at a single point. The presence of both real and imaginary components in the conjugate series signifies that the system is unstable, and this instability is anticipated to result in squealing. The rail–wheel system was designed without considering structural damping.

Table 5: The retrieved complex eigenmodes.

Mode Number	Real Part	Frequency
1	-17.58	1085.7
2	17.58	1085.7
3	-15.96	2312.4
4	15.96	2312.4
5	-11.56	4300.3
6	11.56	4300.3

The scattergram in Figure 10 shows the unstable and stable modes retrieved from the complex eigenvalue analysis. The three unstable modes, marked in red, exhibited instability at frequencies of 1100, 2312, and 4300 Hz.

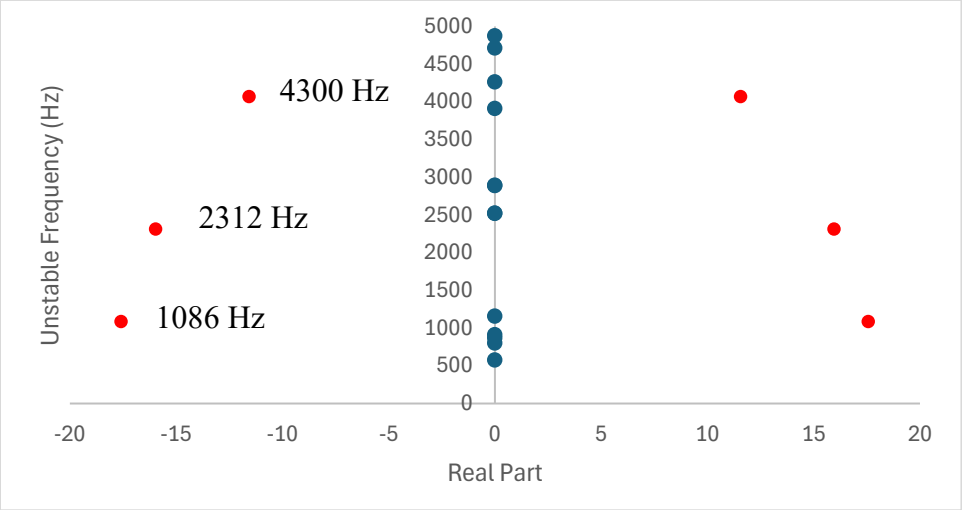

Figure 10: Complex eigenvalue scattergram.

Complex eigenvalue analysis occasionally yields values that are lower than the expected. From Figure 10, it is evident that the initial unstable mode was underestimated at a frequency of 1086

Hz. This is because complex eigenvalue analysis solely considers linear behavior and disregards significant nonlinear effects that contribute to squealing. This can lead to differences from real-world cases that entail dynamic interactions (Fourie et al., 2014; Pieringer et al., 2018). Feng et al. (2024) showed that complex eigenvalue analysis might underestimate the unstable modes owing to the simplified structure of the model and the friction characteristics.

To verify the unstable frequencies acquired, the scattergram was contrasted and validated against the noise spectrum fast Fourier transform (FFT) obtained experimentally from the squeal measurement test using the scaled-down rig, shown in Figure 11. Four frequencies were retrieved in the squeal measurement test. As illustrated in Figure 11, the dominant squeal frequency occurs at 2400 Hz, with additional frequencies noted at 2600 Hz, 4660 Hz, and 6980 Hz. The unstable mode identified at 2312 Hz in the simulation exhibits a close correlation with the dominant squeal frequency of 2400 Hz as recorded experimentally, yielding an error margin of 3.73%. In contrast, the unstable mode at 4300 Hz observed in the simulation corresponds to the third squeal frequency of 4660 Hz, with an error percentage of 13.5%. This is acceptable because the modal analysis confirmed the accuracy. The real part of the eigenvalues of the wheel-rail system, as derived from simulation, verified the frequencies obtained from experimental squeal test. The application of the complex eigenvalue method demonstrates promising results in the identification of unstable modes within the system.

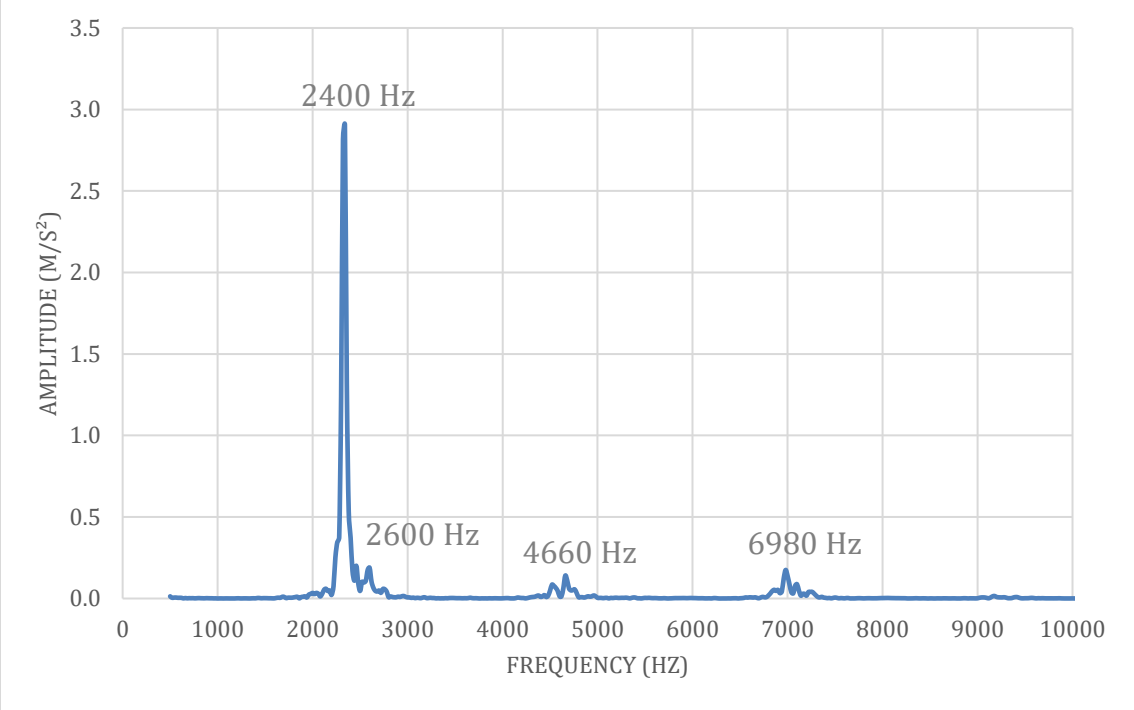

Figure 11: Noise spectrum FFT from squeal test.

3.3 Instability Due To Variations in Friction Coefficient

The impact of friction coefficient on the generation of squeal in the wheel-rail system is evaluated. The friction coefficient was varied from μ = 0.1 to μ = 0.85 with the wheel subjected to a baseline yaw angle of 0.5°.

Figure 12 shows the influence of the friction coefficient and real part of the eigenvalues on the unstable frequencies. The unstable modes begin to appear for friction coefficient μ ≥ 0.35. No instabilities were observed at μ = 0.1 and μ = 0.2. These results are consistent with the observations of Pieringer et al. (2014), indicating that the stick–slip phenomena, which results in system instability, does not occur when the friction coefficient is less than μ = 0.3.

Figure 8 shows that when the friction coefficient reaches μ = 0.35, the real part increases and causes mode coalescence. The two modes at 2450 Hz and 2150 Hz at μ = 0, converged to 2312 Hz at higher μ. Further increasing the friction coefficient did not change the value of the merged frequency. This implies that the wheel–rail system experiences mode coupling, which is the primary factor contributing to the instability of the flutter mechanism in the study of automotive disc brake squeal (Teoh et al., 2013). Our findings exhibit similarities to the previously reported results on automotive brake squeal (Mohd Ripin, 1995; Najib et al., 2013) wherein mode coupling was detected with two distinct modes converging to a common frequency. The yaw angle is the primary cause of mode coupling because the lateral forces acting on the contact point increase with yaw angle. Liu et al. (2023) investigated wheel squeal noise using a two-disk test rig and reported that the likelihood of mode coupling increases with yaw angle. Our findings follow a similar trend and are consistent with the results reported by Ding et al. (2018) who demonstrated that mode coupling is the primary cause of railway curve squeal. The coalescence frequency of 2312 Hz is in good agreement with the experimentally acquired squeal noise at 2400 Hz, as evidenced in the noise spectrum FFT (Figure 11).

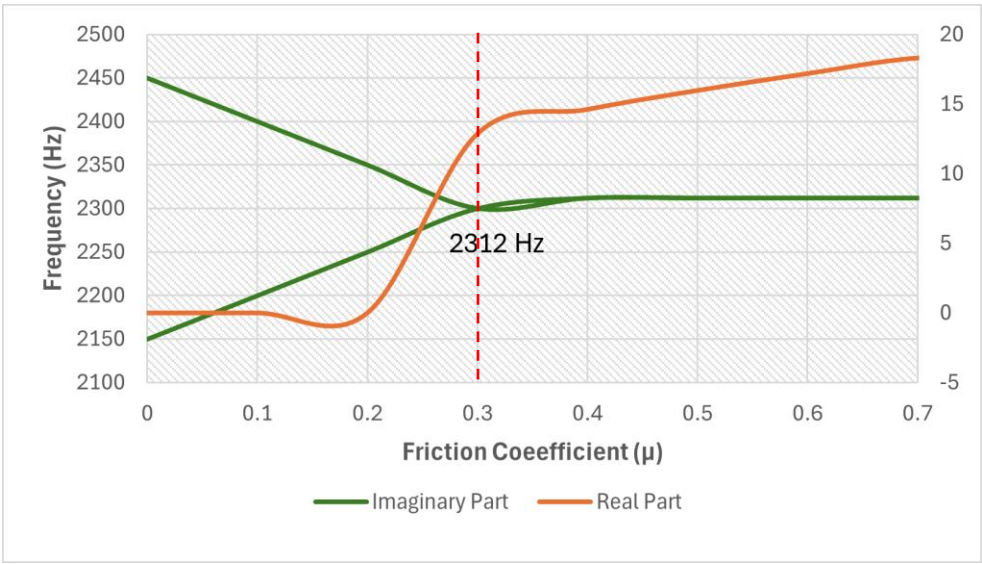

Figure 12: Mode coalescence.

3.4 Instability Due To Variations in Contact Position

Figure 13 shows the structure of the simulated wheel. The regions of the wheel are separated into four segments. Flange, flange root, tread, and field side. Soleimani and Moavenian (2017) indicate that the flange comprises three contact types: single point, dual point, and conformal contact. They assert that single point contact is the most wear-intensive due to concentrated stress and strain at a single area, which deteriorates the wheel and rail (Soleimani & Moavenian, 2017).

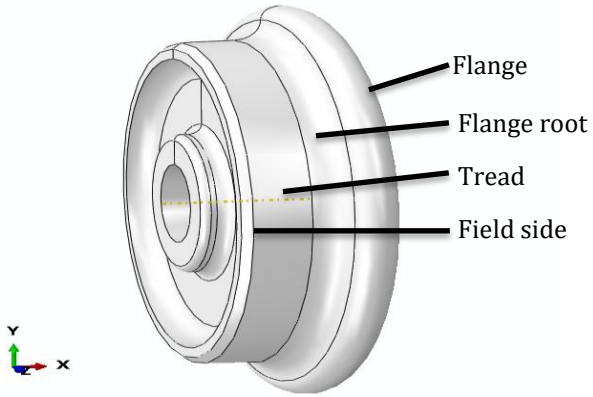

Figure 13: Wheel structure.

To evaluate the impact of the position of the contact point on the wheel–rail interface, which is believed to be a critical parameter for quantifying squeal characteristics, we laterally shifted the contact position on the wheel–rail system. The wheel was laterally shifted to the flange root and the field side from its original location at the tread, as illustrated in Figure 14. This analysis yielded eigenvalues that were then used to evaluate the tendency of squealing

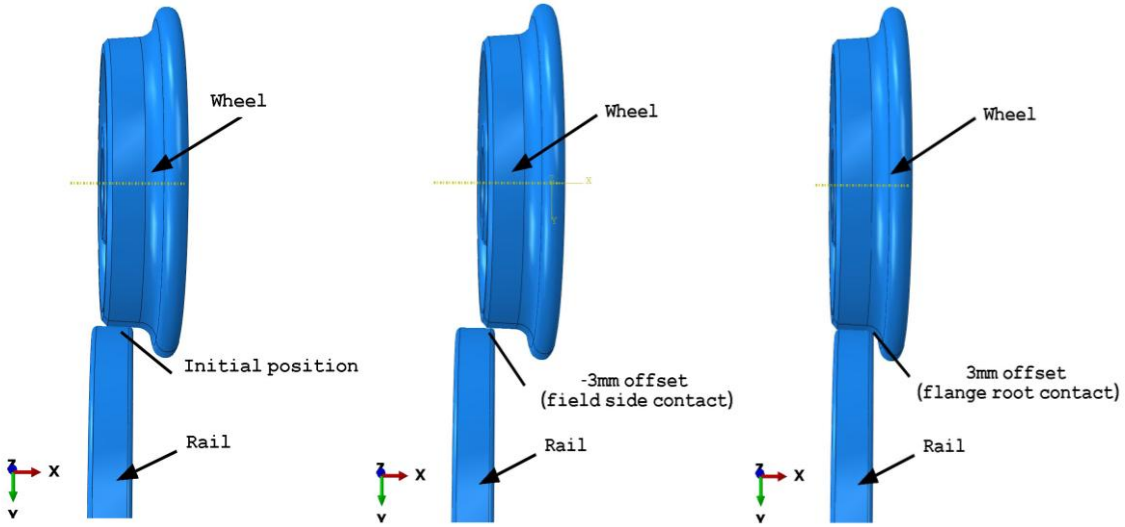

Figure 14: Contact point positions.

Figure 15: shows the cross-section of the rail–wheel system for contact point relocation. The figure displays the von Mises stress, which is linked to the contact pressure. The contact region undergoes a shift when the wheel is laterally displaced from its initial position.

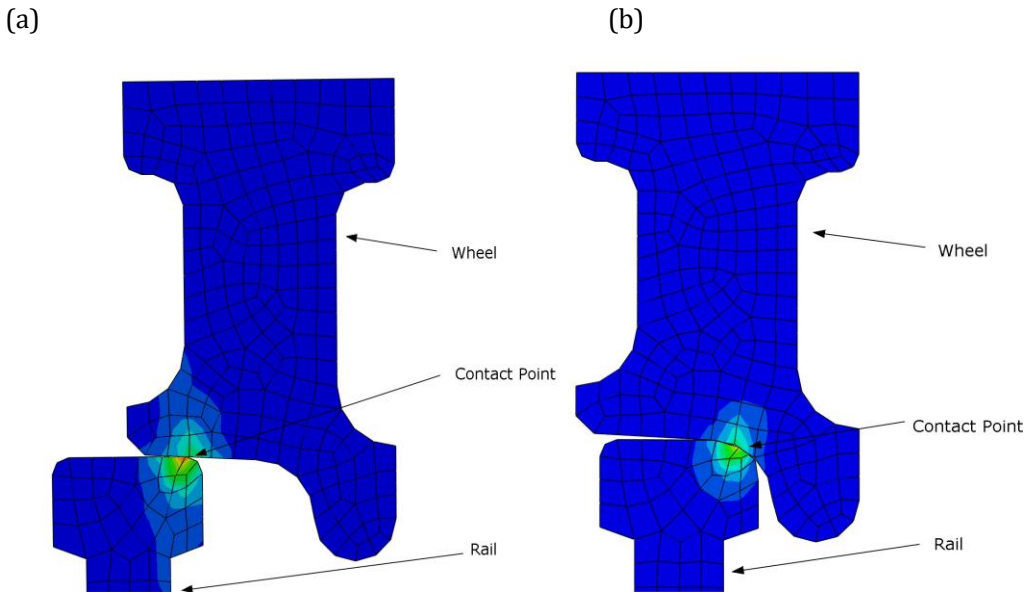

Figure 15: Lateral shift of contact point. (a) Field side; (b) Flange root.

Figure 16 shows the relationship between the real part of the eigenvalues and the observed unstable modes. The location of the contact point significantly influences the generation of self-excited vibrations, which results in squealing.

Figure 16 shows that the positive real part of the eigenvalues increase in magnitude as the initial contact point is laterally shifted by -3 mm towards field side of the wheel. Consequently, the system stability reduces with this shift and an extra unstable mode (shown in red) was identified at a frequency of 4712 Hz. However, when the contact point is moved 3 mm closer to the flange root of the wheel, the real part of the eigenvalues experience a large decrease in magnitude. This demonstrates that laterally adjusting the contact point on the interface between the wheel–rail system can improve the system's stability and decrease the likelihood of squealing. According to Thompson et al. (2009), the location of the contact point on the field side of the tread increases system instability and squeal generation because of higher stress concentration, which in turn increases the lateral forces and tendency of stick-slip.

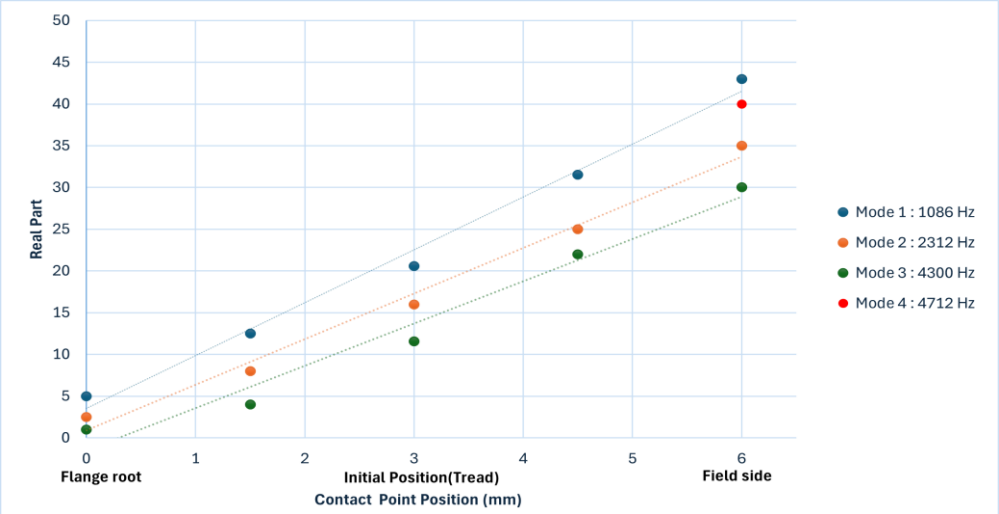

Figure 16: Effect of shifting the contact point.

As demonstrated in Figure 16, the position of the contact point exhibits a significant correlation with the increase in system instability. Quantitatively, the positive real component of the system which serves as a measure of a of instability, increases from a value below 5 at the flange root to 44 at the field side. This observation reflects a ninefold increase from the initial value, thereby augmenting the probability of squealing tendency. The observation that the lateral position of the contact point is a critical parameter in the emergence of instabilities is consistent with the previous studies that showed that relocating the contact patch laterally increases instability.

The asymmetrical geometry of the wheel leads to a greater mode coupling between the normal and tangential dynamics in comparison to the centered position (Van et al., 2019). Our findings are consistent with those of Zenzoric et al. (2016) who determined that the contact position at the field side is more susceptible to generating squealing due to the significant impact of the vertical–lateral dynamics of the system. These dynamics play a crucial role in determining the strength of geometric coupling and the specific wheel mode that induces squealing. Pieringer et al. (2024) showed that contact points located on the field side of the wheel lead to instability in the wheel–rail system, and that lateral contact forces exerted on the field side of the wheel are significantly greater than those on the flange root of the wheel.

Figure 17 shows the contact patch on the field side (a) and the flange root (b) of the wheel. The maximum contact pressure attained at the field side is 767 MPa, which is significantly higher than the contact pressure of 399 MPa at the wheel's flange root. This analysis demonstrates that the contact pressure at the field side is higher than the contact pressure at the flange root. Wang et al. (2022) demonstrated that a negative yaw angle, coupled with minimal lateral displacement, can result in exacerbated wear effects, as an increase in contact pressure was observed when the yaw angle was adjusted in the negative direction in their investigation. The contact patch in this analysis is elliptical, suggesting a hertzian contact that is consistent with the findings of (Singh & Ripin, 2023).

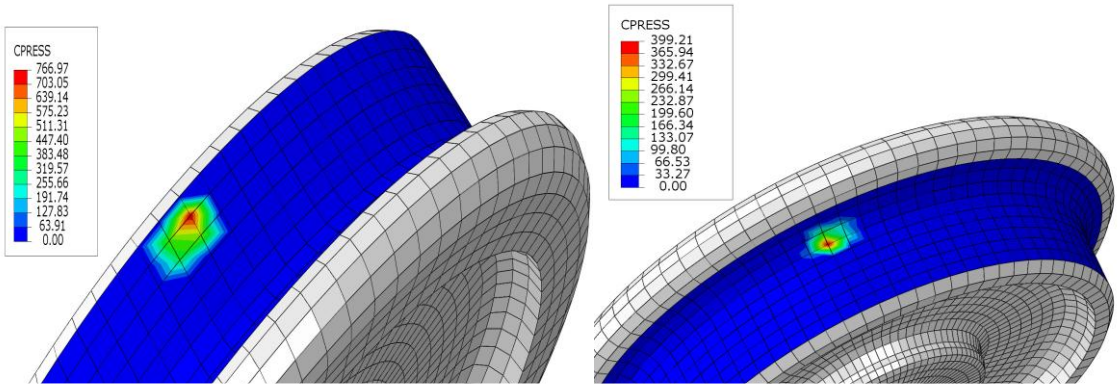

(a) (b)

Figure 17: Maximum contact pressure at field side (a) and flange root (b).

The maximum von Mises stress reached 772 MPa on the field side of the wheel, attributed to shear stress in both lateral and vertical orientations, significantly exceeding the set yield stress of 545 MPa. This stress can cause accelerated wear and surface corrugations which will lead to instability of the system, which is consistent with the findings of Aalami et al. (2013) who reported that von Mises stress above 550 MPa leads to increased wear. Goo and Kim (2016) observed that von Mises stress is contingent upon the coefficient of friction, noting that von Mises stress escalates with the introduction of friction into the system. The elevation of friction coefficients results in elevated contact stress, which induces the slip phase of the stick-slip phenomenon observed in the tribological performance of a tire block (Setiyana, 2024).

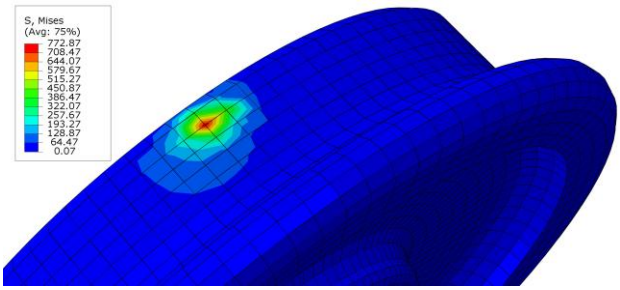

Figure 18: Maximum von Mises stress at field side.

The unstable mode shapes when the contact position is shifted laterally towards the field side of the wheel, shown in Figure 19. The mode shapes closely resembled the natural frequencies of both the rail and the wheel. No unstable modes were observed above 5000 Hz. As explained in section 2.1.1, although finer meshing can effectively capture stress levels, it requires substantial computational resources and time for simulation. Therefore, a mesh size of 0.6 mm is selected as optimal.

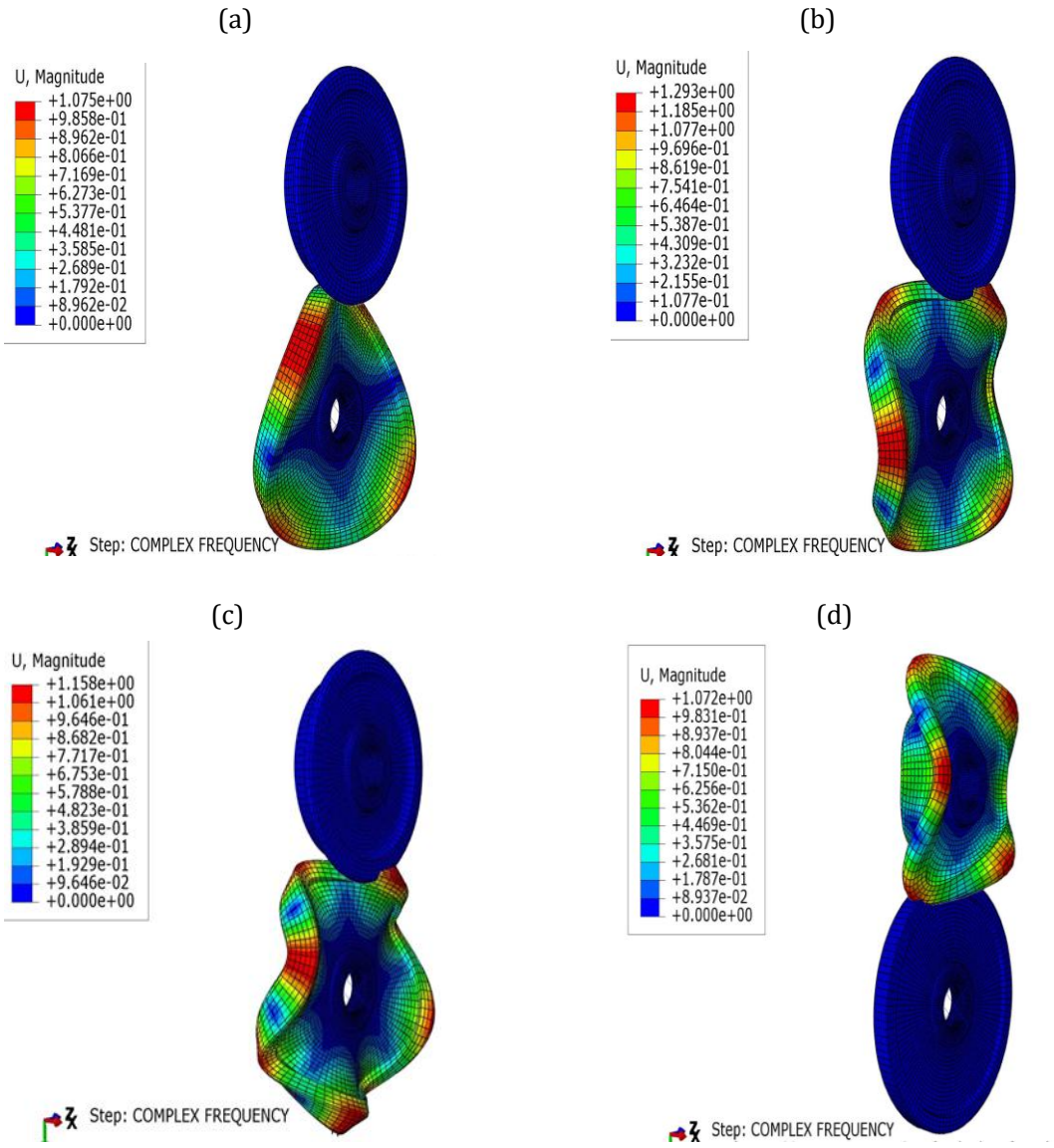

Figure 19: Unstable mode shapes of the rail–wheel system at (a) 1086 Hz, (b) 2312 Hz, (c) 4300 Hz, and (d) 4712 Hz.

3.5 Instability Due To Variations in Preloading

To simulate the effect of radius of curvature, the wheel–rail system was subjected to a baseline concentrated force in both the vertical and lateral directions as described in Section 2.1.2. The system was preloaded to ensure comparable stress levels in both the normal direction and lateral directions. The effects of radius curvature can be replicated by rotating the wheel about its vertical axis (Y-axis) and applying lateral force on the rail. The impact of vertical preloading and lateral preloading is contrasted in figure 20. The scatterplot indicates that vertical preloading

does not completely exacerbate the system's stability, whereas lateral preloading significantly increases the real part of the eigenvalues, indicating greater instability. When lateral preload is applied, unstable frequencies of up to 8000 Hz were detected.

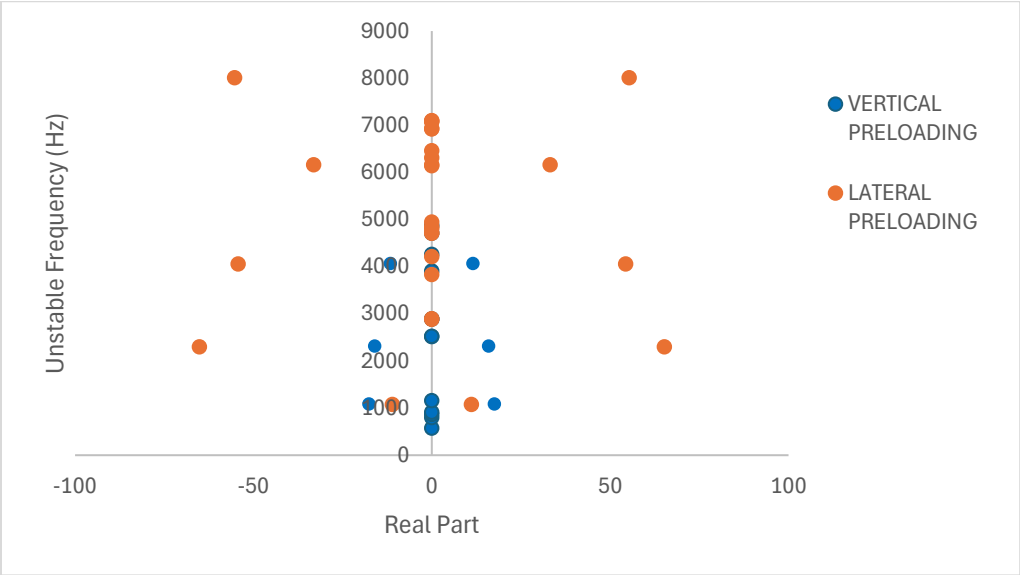

Figure 20: Simulated preloading instability scattergram.

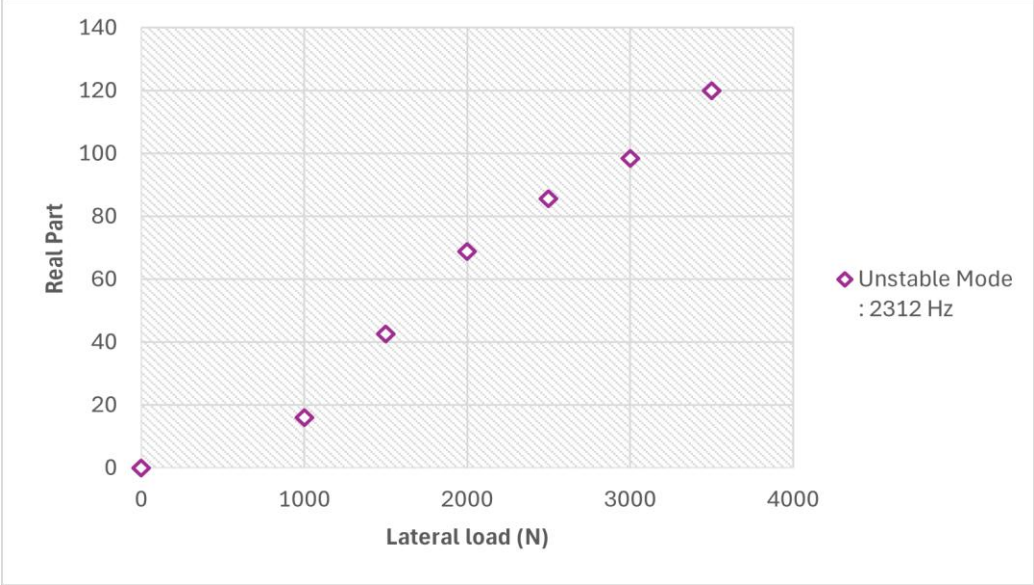

Figure 21: Simulated effects of lateral preloading.

To simulate the effect of radius of curvature, wheel-rail system was preloaded in the lateral direction and the concentrated force was varied from 1000 N to 3000 N to mimic the curvature effect. Figure 21 shows the effect of varying the lateral preload. As the lateral preload increases,

the positive real part (for unstable frequency 2312 Hz), which denotes the instability of the system, increases significantly, showing that the system becomes more unstable as the radius of curvature increases.

The wheel was then rotated about its vertical axis by varying the yaw angle from 0.5° to 3° to further corroborate whether increasing the radius of curvature induces instability. Figure 18 shows that the contact pressure and the positive real part for the 2312 Hz unstable mode increase with the yaw angle, showing that the system gets more unstable as the yaw angle increases. Additionally, it is evident that the maximum contact pressure of 680 MPa was achieved when the yaw angle was set to 3°, while the maximum contact pressure of 250 MPa was achieved when the baseline yaw angle of 0.5° was used. This implies that the yaw angle resulted in an increase in contact pressure, which further exacerbated the system's instability, as demonstrated by the increase in the real part.

The results obtained in Figure 22 demonstrate a comparable trend to a study conducted by Yun and Kim (2021), which indicated that as the yaw angle increases, the adhesion coefficient decreases due to lateral creepage induced by the yaw angle. It was also noted as the yaw angle increases, the sound pressure level increases sharply, leading to the occurrence of squeal (Yun & Kim, 2021). As supported by Liu et al. (2023), increase in yaw angle from 10mrad to 15mrads increases the squeal noise level increased significantly as demonstrated in his findings using a twin disk rig. Similarly, as indicated by C. Wang (2015), an increase in yaw angle due to lateral creepage showed an increase in real part of eigenvalue thus it can be implied that the yaw angle plays a major role in causing instability that will manifest as squeal. As demonstrated by Ngamkhanong et al. (2018), a low radii radius of curvature ranging from 100m to 200m showed increased in lateral displacement from 0.1mm to 0.75mm which indicated a 78% increase in lateral displacement and implied that lateral displacement which is a lateral creepage responses are more sensitive corresponding to low radii, which gave evidence on the appearance of squeal during train negotiating tight curves (Ngamkhanong et al., 2018).

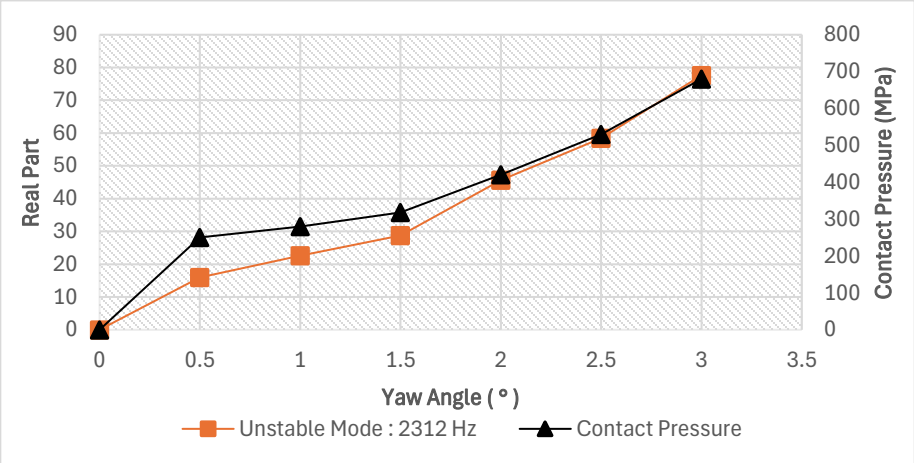

Figure 22: Simulated effects of yaw angle.

CONCLUSIONS

This study performed curve squeal analysis of a train traversing a curved track. The dynamic behavior while negotiating a curve was investigated by simulating the wheel–track interaction under rolling conditions and imposing lateral preloading with a baseline yaw angle to reproduce the effect of curvature. Stability analysis was performed using the complex eigenvalue method to extract the unstable modes. The dominant squeal of 2400 Hz observed from the experimental squeal measurement corresponded well with the unstable modes, specifically at 2312 Hz and 4300 Hz from the stability analysis, therefore validating the twin-disk rig. No unstable modes were identified for $\mu < 0.35$. The real part increased with the friction coefficient, and mode coupling was observed as two unstable frequencies (2450 Hz and 2150 Hz at $\mu = 0$) converged to 2312 Hz at $\mu \geq 0.3$. The contact point's position, particularly at the field side of the wheel was observed to increase the real part of the system significantly, hence exacerbating the instability. Besides that, the wheel experienced significant instability when preloaded laterally, with a twofold increase in the real part of the eigenvalues in comparison to that under vertical preloading.

ACKNOWLEDGEMENT

This research was funded by a research grant (304.PMEKANIK.6050379) Universiti Sains Malaysia

REFERENCES

Aalami, M. R., Anari, A., Shafighfard, T., & Talatahari, S. (2013). A robust finite element analysis of the rail-wheel rolling contact. Advances in Mechanical Engineering, 5, 272350.

Anyakwo, A. (2020b). Condition monitoring of curve squeal based on analysis of acoustic and vibration data (By University of Huddersfield). http://eprints.hud.ac.uk/id/eprint/35286/

Beshbichi, O. E., Wan, C., Bruni, S., & Kassa, E. (2020). Complex eigenvalue analysis and parameters analysis to investigate the formation of railhead corrugation in sharp curves. Wear, 450, 203150.

Chen, G. X., Xiao, J. B., Liu, Q. Y., & Zhou, Z. R. (2008). Complex eigenvalue analysis of railway curve squeal. In B. Schulte-Werning et al. (Eds.), Noise and Vibration Mitigation for Rail Transportation Systems. Notes on Numerical Fluid Mechanics and Multidisciplinary Design, Springer, pp. 415-423.

Chen, G. (2020). Friction-Induced Vibration of a Railway Wheelset-Track System and Its Effect on Rail Corrugation. Lubricants, 8(2), 18. https://doi.org/10.3390/lubricants8020018.

de Beer, F. G., Janssens, M. H. A., & Kooijman, P. P. (2003). Squeal noise of rail-bound vehicles influenced by lateral contact position. Journal of Sound and Vibration, 267, 497–507.

Ding, B. (2018). The mechanism of railway curve squeal. PhD Thesis, University of Southampton.

Ding, B., Squicciarini, G., Thompson, D., & Corradi, R. (2018). An assessment of mode-coupling and falling-friction mechanisms in railway curve squeal through a simplified approach. Journal of Sound and Vibration, 423, 126–140.

Du, Y., & Wang, Y. (2017). Squeal analysis of a modal-parameter-based rotating disc brake model. International Journal of Mechanical Sciences, 131–132, 1049–1060.

Eriksson, M., & Jacobson, S. (2001). Friction behaviour and squeal generation of disc brakes at low speeds. In Proceedings of the Institution of Mechanical Engineers, Part D: Journal of Automobile Engineering, pp. 1245–1256.

Feng, X., Chen, G., Song, Q., Dong, B., & Ren, W. (2024). A root cause of curve squeal: Self-excited frictional vibration of a wheelset–track system. Journal of Tribology, 146(6), 061501.

Fourie, D., Gräbe, P., Heyns, P., & Fröhling, R. Analysis of railway wheel-squeal due to unsteady longitudinal creepage using the complex eigenvalue method. In Proceedings of the 10th International Conference on Contact Mechanics and Wear of Rail/Wheel Systems, pp. 57–69.

Gao, Y., Zhang, G., Yuan, M., Ji, J., Cui, N., & Huang, S. (2023). The numerical study for the effect of stiffness matching on wheel–rail curve squeal noise. Applied Sciences, 13(21), 11615.

Ghani, J. A., Ismanizan, M. A., Rahman, H. A., Haron, C. H. C., Juri, A. Z., Kasim, Mohd. S., & Rizal, M. (2024). Machining analysis of S45C carbon steel using finite element method. Jurnal Tribologi, 40, 226–246.

Glocker, Ch., Cataldi-Spinola, E., & Leine, R. I. (2009). Curve squealing of trains: Measurement, modelling, and simulation. In M. P. Cartmell (Ed.), Journal of Sound and Vibration, pp. 365–386.

Goo, B., & Kim, J. (2016). Complex eigenvalue analysis of railway wheel/rail squeal. International Journal of Engineering, Science and Technology, 8(1), 1–12.

Goo, B. C. (2014). Finite element analysis of wheel/rail squeal noise. WIT Transactions on the Built Environment, 1, 217–225.

Hamid, M. N. A., Teoh, C., & Mohd Ripin, Z. (2013). The operational deflection shapes and transient analysis of the brake shoes in drum brake squeal. In Proceedings of the Institution of Mechanical Engineers. Part D, Journal of Automobile Engineering, pp. 866–884.

Han, J., Wei, Y., & Yang, T. (2024). Influence of sliding wear on contact characteristics based on 3-D wheel/rail contact model. Journal of Mechanical Engineering, Automation and Control Systems, 5(1), 1–9.

Hanson, D., Jiang, J., Dowdell, B., & Dwight, R. (2014). Curve squeal: Causes, treatments, and results. In Proceedings of Inter-noise 2014. Transport for New South Wales Freight & Regional Development, Australia; CRC for Rail Innovation, University of Wollongong, Australia.

Heckl, M. A., & Abrahams, I. (2000). Curve squeal of train wheels, part 1: Mathematical model for its generation. Journal of Sound and Vibration, 229(3), 669–693.

Hidayat, T., Ismail, R., Tauviqirrahman, M., Saputra, E., Ammarullah, M. I., Lamura, M. D. P., Bayuseno, A. P., & Jamari, J. (2023). Investigation of mesh model for a finite element simulation of the dual-mobility prosthetic hip joint. Jurnal Tribologi, 38, 118–140.

Hsu, S. S., Huang, Z., Iwnickl, S. D., Thompson, D. J., Jones, C. J. C., Xie, G., & Allen, P. D. (2007). Experimental and theoretical investigation of railway wheel squeal. In Proceedings of the Institution of Mechanical Engineers, Part F: Journal of Rail and Rapid Transit, Special Issue Paper, pp. 59–73.

Huang, Z. (2007). Theoretical modelling of railway curve squeal. PhD Thesis, University of Southampton.

Inoue, H., & Kamada, T. (2020). Structural instability of friction-induced vibration by characteristic polynomial plane applied to brake squeal. Journal of Advanced Mechanical Design, Systems, and Manufacturing, 14(1), JAMDSM0014.

Joe, Y.-G., Cha, B.-G., Sim, H.-J., Lee, H. J., & Oh, J. E. (2008). Analysis of disc brake instability due to friction-induced vibration using a distributed parameter model. International Journal of Automotive Technology, 9, 161–171.

Kinkaid, N. M., O'Reilly, O. M., Papadopoulos, P. (2003). Automotive disc brake squeal. Journal of Sound and Vibration, 267, 105–166.
Koch, J., Vincent, N., Chollet, H., & Chiello, O. (2006). Curve squeal of urban rolling stock—Part 2: Parametric study on a 1/4 scale test rig. Journal of Sound and Vibration, 293(3–5), 701–709.
Lai, V.-V., Chiello, O., Brunel, J.-F., & Dufrenoy, P. (2019). Full finite element models and reduction strategies for the simulation of friction-induced vibrations of rolling contact systems. Journal of Sound and Vibration, 444, 197–215.
Lee, C.-W., & Kim, J.-C. (2011). Influence of the speeds on the curve squeal noise of railway vehicles. Journal of the Korean Society for Precision Engineering, 28(5).
Liu, S., De Silva, U., Chen, D., Leslie, A. C., & Meehan, P. A. (2023). Investigation of wheel squeal noise under mode coupling using two-disk test rig experiments. Wear, 530–531, 205035.
Liu, X., & Meehan, P. A. (2013). Investigation of the effect of lateral adhesion and rolling speed on wheel squeal noise. In Proceedings of the Institution of Mechanical Engineers, Part F: Journal of Rail and Rapid Transit, pp. 469–480.
Ma, K., & Yang, X. (2024). Analysis of the Mechanism of Rail Corrugation by Using Temperature Dependent Friction Coefficient. In Lecture notes in mechanical engineering (pp. 285–294). https://doi.org/10.1007/978-981-99-7852-6_26.
Meehan, P. A. (2019). Prediction of wheel squeal noise under mode coupling. Journal of Sound and Vibration, 465, 115025.
Mohd Ripin, Z. B. (1995). Analysis of disc brake squeal using the finite element method, PhD Thesis, University of Leeds.
Monk-Steel, A. D., Thompson, D. J., de Beer, F. G., & Janssens, M. H. A. (2006). An investigation into the influence of longitudinal creepage on railway squeal noise due to lateral creepage. Journal of Sound and Vibration, 293, 766–776.
Münzel, T., Molitor, M., Kuntic, M., Hahad, O., Röösli, M., Engelmann, N., Basner, M., Daiber, A., & Sørensen, M. (2024). Transportation noise pollution and cardiovascular health. Circulation Research, 134(9), 1113–1135.
Ngamkhanong, C., Liu, X., & Kaewunruen, S. (2018). Nonlinear dynamic lateral responses of curved railway track associated with high-frequency squeal noises. In 13th World Congress on Computational Mechanics (WCCM XIII) (pp. 1878-1886). United States Association for Computational Mechanics. http://www.wccm2018.org/sites/default/files/WCCM2018-Abstracts.pdf.
Pieringer, A. (2014). A numerical investigation of curve squeal in the case of constant wheel/rail friction. Journal of Sound and Vibration, 333(18), 4295–4313.
Pieringer, A., Torstensson, P. T., & Giner, J. (2016). Curve squeal of rail vehicles: Linear stability analysis and non-linear time-domain simulation. In Proceedings of the 3rd International Conference on Railway Technology: Research, Development and Maintenance, pp. 1759–3433.
Pieringer, A., Torstensson, P. T., Giner, J., & Baeza, L. (2018). Investigation of railway curve squeal using a combination of frequency- and time-domain models. In Anderson, D. et al. (Eds.), Noise and Vibration Mitigation for Rail Transportation Systems, Notes on Numerical Fluid Mechanics and Multidisciplinary Design, Springer, Cham, 139, 5.
Pieringer, A., Torstensson, P., Theyssen, J., & Kropp, W. (2024). Transient modelling of curve squeal considering varying contact conditions. In Sheng, X. et al. (Eds.), Noise and Vibration Mitigation for Rail Transportation Systems, IWRN 2022, Lecture Notes in Mechanical Engineering, Springer, 1-15.

Rudd, M. J., & Bolt Beranek and Newman Inc. (1976). Wheel/rail noise—Part II: Wheel squeal. Journal of Sound and Vibration, 46(3), 381–394.

Rusli, M., Fesa, M., Dahlan, H., & Bur, M. (2020). Squeal noise analysis using a combination of nonlinear friction contact model. International Journal of Automotive Mechanical Engineering, 17(3), 8160–8167.

Sueki, T., Shimizu, Y., & Nitta, T. (2022). Study on squeal noise generated in curved sections of railways. In Proceedings of the Symposium on Environmental Engineering, pp. 1105–1103.

Soleimani, H., & Moavenian, M. (2017). Tribological Aspects of Wheel–Rail Contact: A Review of Wear Mechanisms and Effective Factors on Rolling Contact Fatigue. Urban Rail Transit, 3(4), 227–237.

Singh, C., & Ripin, Z. M. (2023). Static analysis of railway curve squeal using the finite element method. AIP Conference Proceedings, 2959, 050003.

Setiyana, B., 1. (2024). The tribological performance identification of a tire tread block during friction contact: A numerical investigation. In University of Diponegoro, University of Twente, & State Polytechnic of Semarang, Jurnal Tribologi (Vol. 41, pp. 81–92).

Teoh, C., Mohd Ripin, Z., & Hamid, M. N. A. (2013). Analysis of friction excited vibration of drum brake squeal. International Journal of Mechanical Sciences, 67, 59–69.

Thompson, D., & Thompson, D. J. (2009). Railway noise and vibration: Mechanisms, modelling and means of control. Elsevier Science.

Thompson, D. J., Squicciarini, G., Ding, B., & Baeza, L. (2018). A state-of-the-art review of curve squeal noise: phenomena, mechanisms, modelling and mitigation. In Anderson, D., et al. (Eds.), Noise and Vibration Mitigation for Rail Transportation Systems, Notes on Numerical Fluid Mechanics and Multidisciplinary Design, Springer, 1-9.

Vincent, N., Koch, J., Chollet, H., & Guerder, J. (2006). Curve squeal of urban rolling stock—Part 1: State of the art and field measurements. Journal of Sound and Vibration, 293(3–5), 691–700.

Valente, L., Lopes, L., & Ribeiro, L. S. (2023). Influence of Bogie Maintenance and Retrofitting on Wheel Wear: Analysis Using Integer Programming and Multibody Simulation. Applied Sciences, 13(10), 6101. https://doi.org/10.3390/app13106101.

Wang, Q., Huang, X., Wang, J., Ni, Y., Ran, S., Li, J., & Zhang, J. (2024). Concise Historic Overview of Rail Corrugation Studies: From Formation Mechanisms to Detection Methods. Buildings, 14(4), 968. https://doi.org/10.3390/buildings14040968.

Wang, C. (2015). Wheel rail curve squeal modeling & rolling stock based mitigation measures [Master of Philosophy thesis, University of Wollongong]. https://ro.uow.edu.au/theses/4953.

Wu, J., Grande, G., Pyko, A., Laukka, E. J., Pershagen, G., Ögren, M., Bellander, T., & Rizzuto, D. (2024). Long-term exposure to transportation noise in relation to global cognitive decline and cognitive impairment: Results from a Swedish longitudinal cohort. Environment International, 185, 108572.

Yun, Y., & Kim, J. (2021). Reducing Curve Squeal Noise Using Composite Materials Based on Experimental Investigation. International Journal of Precision Engineering and Manufacturing, 22(9), 1573–1582. https://doi.org/10.1007/s12541-021-00540-y.

Zenzerovic, I., Kropp, W., & Pieringer, A. (2016). An engineering time-domain model for curve squeal: Tangential point-contact model and Green's functions approach. Journal of Sound and Vibration, 376, 149–165.